Electronic Supplementary Information (ESI) for

Improved polaronic transport under a strong Mott-Hubbard interaction in Cu-substituted NiO

Seong Gon Park[1†], Kyu Hyoung Lee[2†], Jae-Hoon Lee[1], Ceukchan Bang[1], Junghwan Kim[3], Hee Jung Park[4], Min Suk Oh[5], Suyoun Lee[6], Young-Hoon Kim[7], Young-Min Kim[7], Hideo Hosono[3,8], Joonho Bang[7]*, and Kimoon Lee[1]*

[1]Department of Physics, Kunsan National University, Gunsan 54150, Republic of Korea.

[2]Department of Materials Science and Engineering, Yonsei University, Seoul 03722, Republic of Korea.

[3]Materials Research Center for Element Strategy, Tokyo Institute of Technology, Yokohama 226-8503, Japan.

[4]Department of Materials Science and Engineering, Dankook University, Cheonan 31116, Republic of Korea.

[5]Display Materials and Components Research Center, Korea Electronics Technology Institute (KETI), Seongnam 13509, Republic of Korea.

[6]Center for Electronic Materials, Post-Silicon Semiconductor Institute, Korea Institute of Science and Technology (KIST), Seoul 02792, Republic of Korea.

[7]Department of Energy Science, Sungkyunkwan University (SKKU), Suwon 16419, Republic of Korea.

[8]Materials and Structures Laboratory, Tokyo Institute of Technology, Yokohama 226-8503, Japan.

[†]These authors contributed equally to this work.

*Corresponding author: joonhobang@kunsan.ac.kr, kimoon.lee@kunsan.ac.kr

Table of Contents

S1. Detailed synthetic process chart for Ni$_{1-x}$Cu$_x$O samples

The process chart for Ni$_{1-x}$Cu$_x$O sample preparation is displayed in Figure S1. Full description for the synthetic process can be also shown from “2.1. Material synthesis” section in the main manuscript.

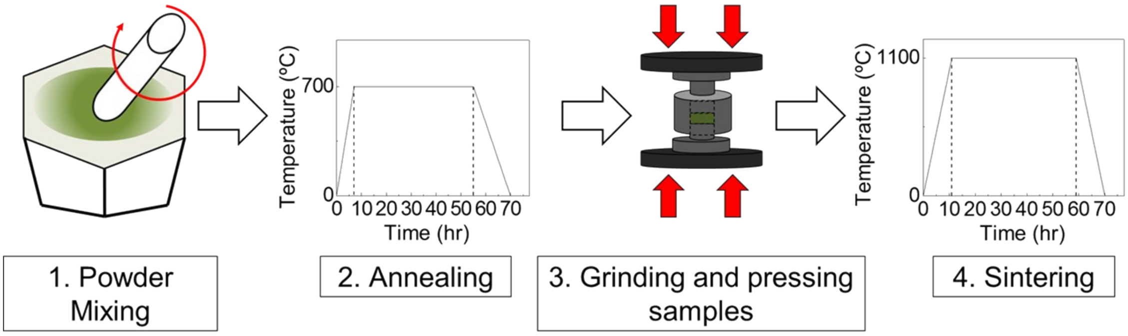

Figure S1. Process chart for the synthesis of sintered Ni$_{1-x}$Cu$_x$O polycrystalline samples.

S2. Determination of stoichiometry of $Ni_{1-x}Cu_xO$ samples

To confirm the exact chemical compositions for $Ni_{1-x}Cu_xO$ samples compared to the nominal values, we performed electron probe micro analyzer (EPMA) measurement. From the atomic composition as listed in TABLE S1, it can be concluded that the measured stoichiometry is almost identical to the nominal one with a little deviation especially for the high concentration of Cu.

TABLE S1. The atomic composition for $Ni_{1-x}Cu_xO$ determined by electron probe micro analyzer (EPMA)

x (nominal)	Ni (at. %)	Cu (at. %)	O (at. %)	x (measured)
0.00	49.4853	0.0544	50.4603	0.00
0.05	46.6515	2.4075	50.9411	0.05
0.10	45.0665	4.5956	50.3379	0.09
0.15	42.1020	7.2737	50.6243	0.14
0.20	40.0814	9.7860	50.1326	0.20
0.25	37.4470	11.8982	50.6548	0.22
0.30	36.8594	13.1548	49.9857	0.26

S3. Detection of Hall voltage from $Ni_{0.78}Cu_{0.22}O$ sample

In general, Hall voltage signal (V_H) is hard to detect when the carrier mobility is too low (< 0.1 cm^2/Vs) through the conventional DC Hall-effect measurement with permanent magnet setup. (< 0.55 T) By adopting excitation current (I_{ex}) sweep technique with applying forward and reverse magnetic field (H), we successfully measure a definite V_H for $Ni_{0.78}Cu_{0.22}O$ sample under an effective H of 1.1 T (twice of 0.55 T applied by commercial Nd-based permanent magnet) which exhibits the lowest electrical resistivity among our synthesized samples. As shown in Figure S2, a linear slope from V_H versus I_{ex} plot can be clearly observed with a relation of [S. O. Kasap, *Electronic Materials and Devices 2nd ed.* McGraw-Hill, New York (2002)]

$$V_H = V_{xy}(H) - V_{xy}(-H) = -\frac{2H}{ent} I_{ex}$$

where $V_{xy}(H)$ is a measured voltage perpendicular to the direction of I_{ex} at H, e is an element electric charge, n is a carrier concentration, and t is the sample thickness. From the positive slope behavior in V_H versus I_{ex} curve, it can be clarified that the majority carrier is hole, and we can estimate n as 1.34×10^{16} cm^{-3}. Finally, the hole carrier mobility (μ) also can be deduced as 0.007 cm^2/Vs with a relation of $\sigma = 1/\rho = ne\mu$ where, σ is electrical conductivity.

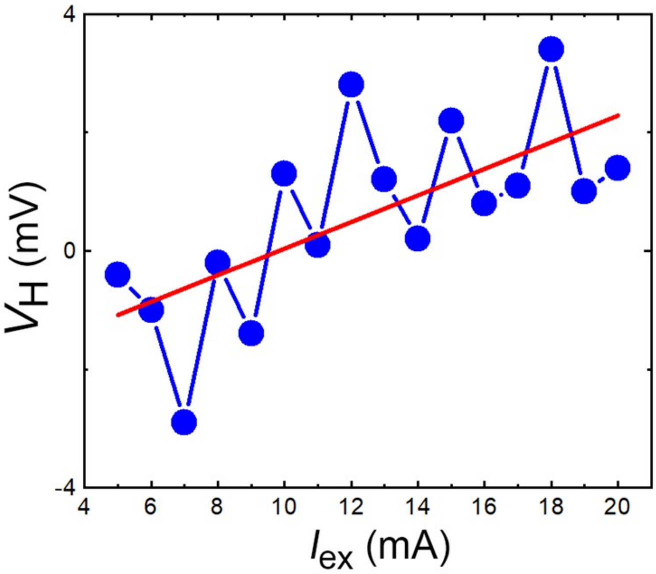

Figure S2. Measured V_H as a function of I_{ex} for $Ni_{0.78}Cu_{0.22}O$ sample. Linear fitting curve is displayed by red-colored line.

S4. Optical properties for $Ni_{1-x}Cu_xO$ samples

Figure S3 shows absorption spectra obtained from the ellipsometry measurement for $Ni_{1-x}Cu_xO$ samples with various x values. To estimate the indirect and direct absorption edges, measured absorption coefficients (α's) are converted into $(\alpha h\nu)^{0.5}$ and $(\alpha h\nu)^2$, respectively, where $h\nu$ is the incident photon energy.

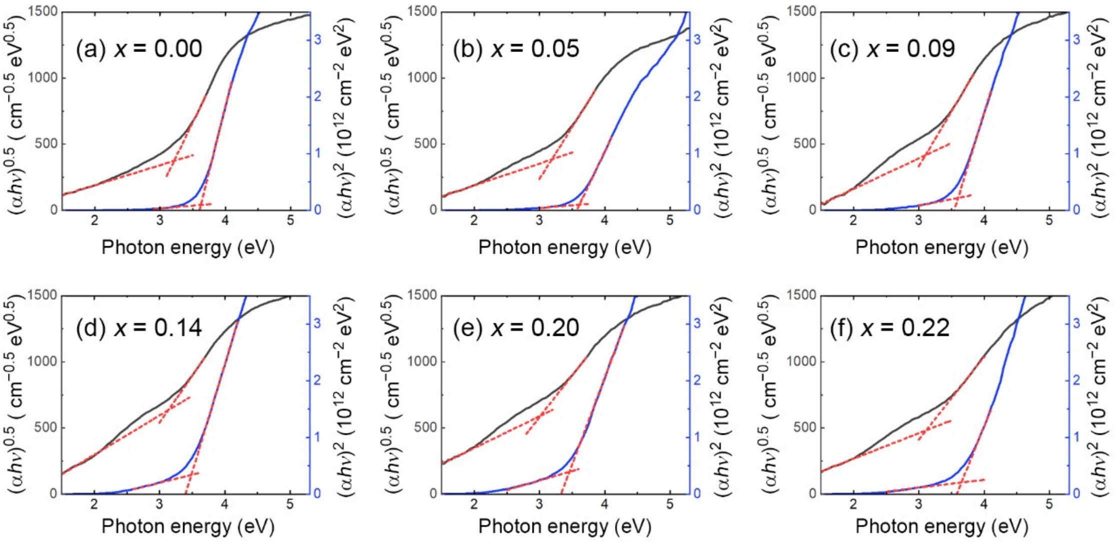

Figure S3. Optical absorption spectra for $Ni_{1-x}Cu_xO$ samples with (a) $x = 0.00$, (b) $x = 0.05$, (c) $x = 0.09$, (d) $x = 0.14$, (e) $x = 0.20$, and (f) $x = 0.22$. All the resultant band gap values are plotted in figure 3b in the main manuscript.

S5. *M–H* curves for $Ni_{1-x}Cu_xO$ samples

Figure S4 shows magnetic susceptibility (χ) versus applied magnetic field (H) curves for $Ni_{1-x}Cu_xO$ samples at T of 50 and 1000 K. As displayed in the figure, all χ values increase linearly as H increases upon the applied magnetic field (H) of 5000 Oe without any observable hysteresis behavior. It strongly indicates that there is no ferromagnetic ordering for all samples.

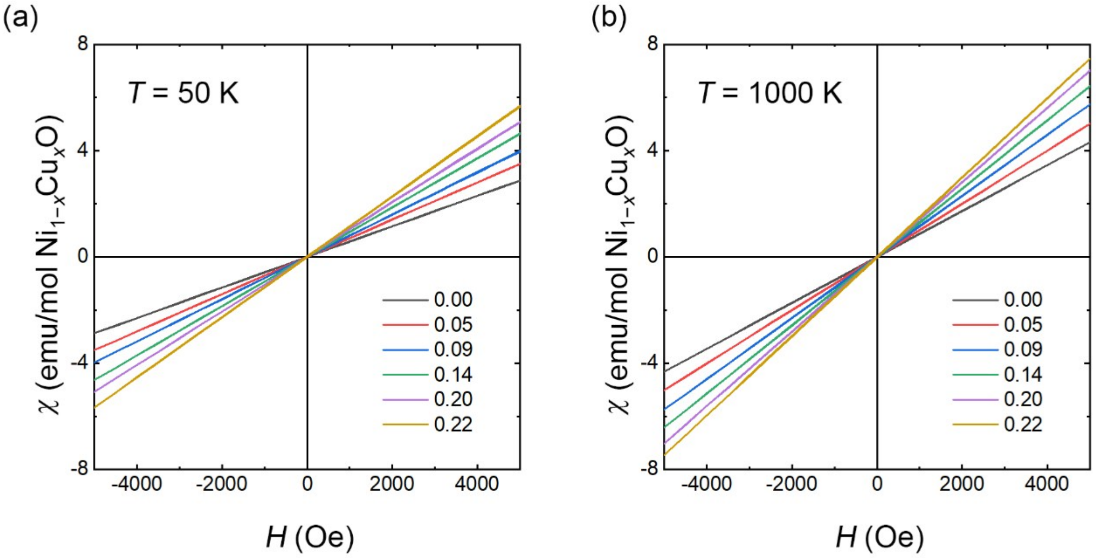

Figure S4. χ versus H curves for $Ni_{1-x}Cu_xO$ measured at (a) $T = 50$ K and (b) $T = 1000$ K.

S6. Supercell structures for density functional theory calculations

For density functional theory (DFT) calculations, we constructed the $2a \times 2b \times 2c$ supercell structure containing 64 atoms as illustrated in Figure S5. (32 Ni and 32 O atoms) By partial replacement of the Ni by Cu atom, the Cu substituted model for $x = 1/32$ is constructed. The calculated lattice parameter was increased from 8.3702 Å for $Ni_{32}O_{32}$ to 8.3754 Å for $Ni_{31}Cu_1O_{32}$, and this trend is consistent with our experimental result from PXRD. (see Figure 1c in the main manuscript)

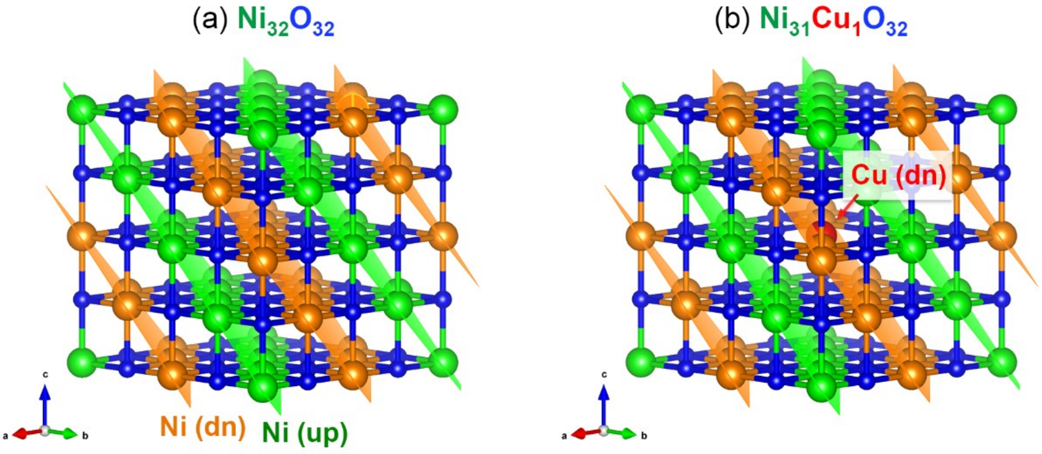

Figure S5. Constructed supercell structures of (a) $Ni_{32}O_{32}$ and (b) $N_{31}Cu_1O_{32}$ for DFT calculations.

S7. X-ray photoemission spectroscopy (XPS) results for $Ni_{1-x}Cu_xO$ samples

We carried out XPS measurements to verify the chemical valence state for Cu impurity in $Ni_{1-x}Cu_xO$ samples. Figure S6a and S6b displays Cu $2p_{3/2}$ core-level spectra for $x = 0.05$ and 0.22 samples. According to Figure S6, Cu^+ states located at 932.6 eV are observed as the main state with both samples, while there also exists a relatively small fraction of Cu^{2+} peak at 934.4 eV. From the fact that Cu impurity mainly substitutes on Ni^{2+}-site in NiO, it confirms that Cu^+-substitution acts as an acceptor, while it exists at a quite deep level position (~0.65 eV above VBM) as shown from our DFT results in Figure 4b.

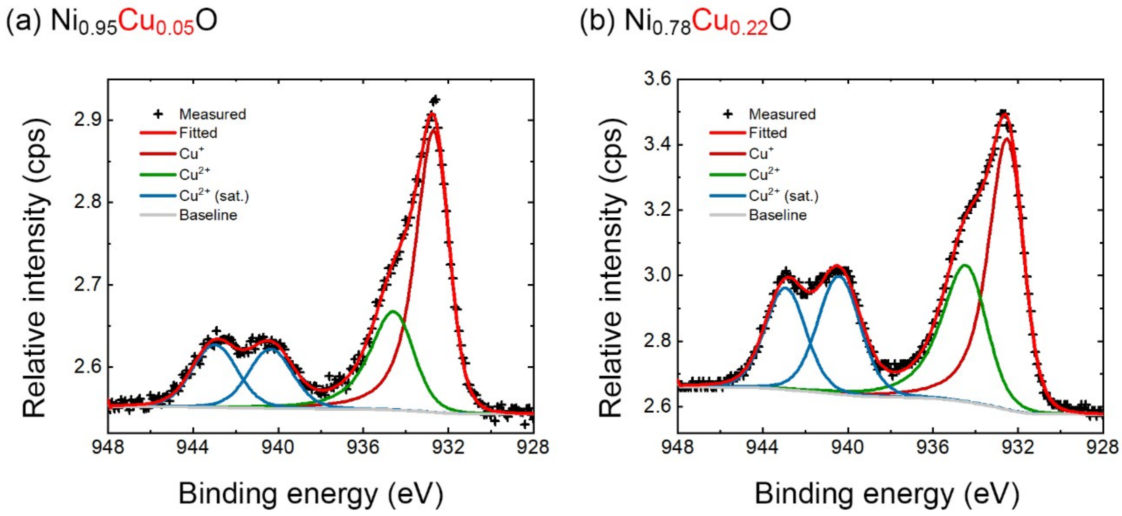

Figure S6. XPS spectra for Cu $2p_{3/2}$ core-level from (a) $Ni_{0.95}Cu_{0.05}O$ and (b) $Ni_{0.78}Cu_{0.22}O$ samples. Cu^+, Cu^{2+} including their satellite peaks are assigned by red, green, and blue Gaussian states, respectively. All atomic spectra were calibrated by taking Au $4f_{7/2}$ peak at 83.96 eV as a reference.